



HAL
open science

Quantum manifestations of Nekhoroshev stability

Daniele Fontanari, Francesco Fassò, Dmitrii A. Sadovskii

► **To cite this version:**

Daniele Fontanari, Francesco Fassò, Dmitrii A. Sadovskii. Quantum manifestations of Nekhoroshev stability. *Physics Letters A*, 2016, 380 (39), pp.3167-3172. 10.1016/j.physleta.2016.07.047 . hal-04218391

HAL Id: hal-04218391

<https://ulco.hal.science/hal-04218391>

Submitted on 3 Oct 2023

HAL is a multi-disciplinary open access archive for the deposit and dissemination of scientific research documents, whether they are published or not. The documents may come from teaching and research institutions in France or abroad, or from public or private research centers.

L'archive ouverte pluridisciplinaire **HAL**, est destinée au dépôt et à la diffusion de documents scientifiques de niveau recherche, publiés ou non, émanant des établissements d'enseignement et de recherche français ou étrangers, des laboratoires publics ou privés.

Quantum manifestations of Nekhoroshev stability

Daniele Fontanari,^{1,*} Francesco Fassò,^{2,†} and Dmitrii A. Sadovskii^{1,‡}

¹*Département de physique, Université du Littoral – Côte d’Opale, 59140 Dunkerque, France*

²*Università di Padova, Dipartimento di Matematica Pura e Applicata, Via Trieste 63, Padova 35121, Italy*

(Dated: imprimé 2015-6-18 at 16:44)

We uncover quantum manifestations of classical Nekhoroshev theory of resonant dynamics using a simple quantum system of two coupled angular momenta with conserved magnitudes which corresponds to a perturbed classical integrable anisochronous model Hamiltonian system.

PACS numbers: 05.45.-a, 45.20.-d, 03.65.-w, 45.20.dc

One of the most influential results of the modern dynamical theory was, arguably, the Kolmogorov–Arnold–Moser (KAM) theorem of the 1960’s on the nonresonant tori of perturbed integrable systems. This theorem provided a firm basis to all studies that relied on integrable approximations to concrete important physical non-integrable systems, such as the Keplerian systems and three-body systems in celestial mechanics and their quantum analogs. One particular KAM result, the persistence in the perturbed system of a dense set of invariant tori, allows, through extrapolation and integrable approximations, extending the torus quantization (known as Einstein-Brillouin-Keller or EBK) to these systems.

In his celebrated study [1, 2], Nekhoroshev developed a complementary approach which allows to characterize both the “regular” or “non-resonant” perturbed dynamics on the persisting KAM tori and—more importantly—the one occurring outside, in the complement of these tori. Following Nekhoroshev, we consider the action space of the original (unperturbed) integrable system and divide it into sector-like zones. Within the nonresonant zones, a nonresonant normal form can be used to approximate the dynamics using a full set of actions whose values are conserved over exponentially long times $\tau \propto e^N$, where N is the highest order of resonance taken into account. This resembles KAM theories. However, with growing perturbation, resonant zones increase in size. Within these zones, KAM tori disappear. Nevertheless, we can still state that during the time τ , the values of the “fast” actions F remain conserved, while on the same time scale, the values of the “slow” actions S evolve slowly (or “drift”) within a small domain.

The theory of exponentially long stability was widely appreciated for explaining the motion of small celestial bodies, such as asteroids, whose motion is strongly affected by low order resonant perturbations due to heavy planets. Furthermore, it gives the best explanation of the stability of the Moon–Earth–Sun system which is perturbed strongly by Jupiter, and more generally, of the stability of the solar system as a whole. In this context, we like to cite classical demonstrations by Laskar and coauthors [3, 4] who sampled their system on a regular grid of initial conditions and detected the non-resonant (or KAM) tori through the respective characteristic frequencies. This lead to a representation of the set of these tori in the frequency space domain, or the frequency map, which is, under

certain conditions, equivalent to an action space map.

Even though resonances of different kinds also play an important—if not a central role in many quantum theories, manifestation of similar dynamics in quantum systems is more difficult. One obvious reason may be that working with long times requires high density of states, especially within the resonance zones. This imposes constraints on the possible quantum systems and requires large computational facilities. Another point, however, seems to deserve attention. With a notable exception of quantum rotors, many popular quantum systems have an integrable approximation, such as a multi-dimensional harmonic oscillator or equivalents, whose Hamiltonian depends linearly on momenta (S^1 actions). These systems are isochronous and their frequency map is degenerate.

One way to overcome these difficulties was to consider non-autonomous periodically driven Hamiltonian systems [5] whose resonances with the driving force can be described by a pendulum approximation [6] similarly to the Nekhoroshev theory. In our work, we decided to consider a model autonomous system suitable for the quantum manifestations of the Nekhoroshev results in their most traditional and simple form. It seems that this idea [7] has been overlooked and yet it produces interesting and enlightening results, important for other studies and applications in concrete systems.

We consider an anisochronous integrable system with, for simplicity, two degrees of freedom, and Hamiltonian H_0 . Its regular dynamics occurs on two-tori labeled by the values of actions I_1 and I_2 . For simplicity, let (I_1, I_2) be global, i.e., let the set of all regular tori Λ be the total space of a trivial fibration over an open domain $A \subset \mathbb{R}^2$, an *action space*, on which H_0 can be written as a function $A \rightarrow \mathbb{R} : (I_1, I_2) \mapsto H_0(I_1, I_2)$. Recall that for an anisochronous system, both frequencies $\omega_k = \partial H_0 / \partial I_k$ with $k = 1, 2$ vary from torus to torus. If we also require convexity, for such systems the *frequency map* $(I_1, I_2) \mapsto (\omega_1, \omega_2)$ is bijective and gives another faithful representation of Λ . Resonances occur when the ratio of (ω_1, ω_2) is rational, i.e., when

$$\nu_1 \omega_1 + \nu_2 \omega_2 = 0, \quad \text{with } \nu = (\nu_1, \nu_2) \in \mathbb{Z}^2.$$

The sets of resonant tori Λ_ν map to curves λ_ν in the action space A . In our case, the latter will be straight lines passing through the origin $(0, 0) \in A$.

As a concrete system, we use two identical symmetric Euler

91 tops coupled through a small perturbation. Its Hamiltonian

$$H = H_0 + \epsilon V = \frac{1}{2}(L_{1z}^2 + L_{2z}^2) + \epsilon V(L_1, L_2) \quad (1)$$

92 depends only on the body-fixed components of the angular
93 momenta L_1 and L_2 whose respective magnitudes L_1 and L_2
94 are conserved and equal $\hbar j = L_1 = L_2$. The small param-
95 eter here is $\hbar\epsilon j$. The nonrigidity and coupling of the rotors is
96 described by the cubic perturbation

$$V = V_{(0,0)} + V_{(1,0)} + V_{(0,1)}, \quad (2)$$

of the principal order ϵ . We have chosen

$$V_{(0,0)} = L_{1z}^3, \quad (3a)$$

$$V_{(1,0)} = 2L_{2z}(L_{2z} - L_{1z})L_{12}, \quad (3b)$$

$$V_{(0,1)} = 4L_{1z}(L_{2z} - L_{1z})L_{22}. \quad (3c)$$

97 The two last terms cause resonances $\nu = (1, 0)$ and $(0, 1)$.
98 We have limited the number of resonances in order to have
99 an example which is both simple and sufficient to explore all
100 essential aspects of the Nekhoroshev theory. These terms are
101 also chosen so that in the next order ϵ^2 , after averaging with
102 respect to the flow of H_0 , they produce only one resonant term
103 with $\nu = (1, 1)$. Note that we have removed all possible sym-
104 metries from the Hamiltonian H in Eq. (1). It is also helpful
105 to assume that the symmetry of H_0 is only $\text{SO}(2) \times \text{SO}(2)$,
106 and that all its other symmetries, such as the invariance with
107 respect to the change in the direction of rotation, are removed.
108 This can be easily achieved explicitly by adding small high
109 degree terms, but the perturbation in Eq. (2) introduces them
110 anyway. The advantage is that in the limit $\epsilon \rightarrow 0$, quantum
111 eigenfunctions will unambiguously become eigenfunctions of
112 \hat{L}_{1z} and \hat{L}_{2z} representing traveling waves $\exp(im\varphi)$ on \mathbb{S}^2
113 and the quantities represented by \hat{L}_{1z} and \hat{L}_{2z} are thus di-
114 rectly observable.

115 The phase space of our system is the product of two spheres
116 $\mathbb{S}^2 \times \mathbb{S}^2$. Its compactness facilitates quantum mechanical cal-
117 culations because the required basis is finite. Specifically, the
118 system of two rotors with Hamiltonian H in Eq. (1) is quan-
119 tized in the standard way using the $\mathfrak{so}(3) \times \mathfrak{so}(3)$ algebra of
120 angular momentum operators \hat{L}_1 and \hat{L}_2 , and its eigenstates
121 are found by diagonalizing $H(\hat{L}_1, \hat{L}_2)$ in the basis of $(2j+1)^2$
122 spherical harmonics $|j, m_1\rangle|j, m_2\rangle$. Many physical interpre-
123 tations of this system can be suggested. In addition to inter-
124 acting spins and rotating particles, we like to mention specific
125 perturbations of the hydrogen atom in the n -shell approxima-
126 tion, and interacting resonant double degenerate vibrations of
127 nuclei or molecules, notably bending vibrations of acetylene
128 or, even better, of its homologue N–C–N.

129 Notice that classical actions

$$I_1 = L_{1z} \quad \text{and} \quad I_2 = L_{2z} \quad (4)$$

130 are not defined globally as the respective conjugate angles are
131 undefined at the poles of $\mathbb{S}^2 \times \mathbb{S}^2$. However, the set of all reg-
132 ular tori Λ of the simple unperturbed integrable system with

133 Hamiltonian H_0 can be represented faithfully using the val-
134 ues of (I_1, I_2) as a square $A \subset \mathbb{R}^2$ (cf Fig. 1) and this is
135 sufficient for our purpose. [We are not interested in what may
136 happen near and at ∂A where (I_1, I_2) cannot serve as action
137 variables.]

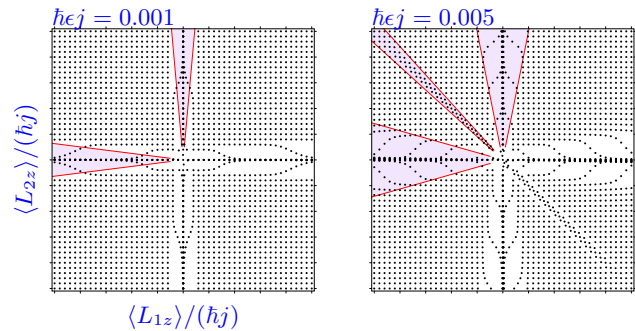


FIG. 1. Joint expectation value spectrum of \hat{L}_{1z} and \hat{L}_{2z} on the eigenstates of the quantum analog of the Hamiltonian in Eq. (1) (dots) and classical resonance zones (wedges) for $j = 25$.

TABLE I. Canonical slow–fast actions S_0 and F , recentered action S , and the threshold parameter b_ν for the resonances ν of our system.

ν	S_0	F	S	b_ν
$(1, 0)$	I_1	I_2	I_1	2ϵ
$(0, 1)$	I_2	$-I_1$	I_2	4ϵ
$(1, 1)$	I_1	$I_2 - I_1$	$(I_1 + I_2)/2$	$6\epsilon^2$

138 In the quantum case, basic information on the behavior of
139 I_1 and I_2 is given by the expectation values $\langle \hat{L}_{1z} \rangle$ and $\langle \hat{L}_{2z} \rangle$.
140 For the $\text{SO}(2) \times \text{SO}(2)$ symmetric unperturbed system these
141 values form a regular lattice in A . In the full system, as we can
142 see in Fig. 1, this lattice is destroyed along the lines of classi-
143 cal resonances ν . The two order- ϵ resonances are clearly seen
144 near axes $I_1 = 0$ and $I_2 = 0$, while the order- ϵ^2 resonance is
145 visible for large values of ϵ along the diagonal $I_1 + I_2 = 0$.
146 It can be conjectured that the wedge-like domains without the
147 lattice are *quantum resonance zones*. The picture is strikingly
148 similar to the classical frequency maps [3, 4] of which, as we
149 explain below, it is indeed a direct quantum analog.

150 Containment of the variation of deformed actions (I_1, I_2)
151 over the exponentially long time τ to the ϵ -neighborhood of
152 their original value, as predicted by the Nekhoroshev theo-
153 rem, means that (L_{1z}, L_{2z}) remain good quantum numbers
154 for those quantum states that correlate with nonresonant tori.
155 Such states continue to be represented by the regular lattice
156 in the joint expectation value spectrum (Fig. 1). Note that by
157 a standard discrete Fourier transform argument for $\mathbb{S}^2 \times \mathbb{S}^2$, it
158 may even follow, that τ remains beyond our time horizon for
159 our value of j and the argument becomes stronger.

160 To understand what happens to the resonant states, i.e.,
161 those for which $(\langle L_{1z} \rangle, \langle L_{2z} \rangle)$ collapse to/near the lines of
162 resonances λ_ν in A , we introduce slow–fast actions (called so
163 after the values of the respective frequencies) for each reso-

nance ν of our system, see Table I. Note that $|F|$ increases as we move along the resonances λ_ν away from 0, while S varies in the orthogonal direction to λ_ν . Since the value of the fast action F should remain conserved over τ , F is a good quantum number and, since F varies along λ_ν , we should have a regular periodic pattern in the zone around λ_ν labeled approximately by $\langle F \rangle$. That is precisely what we observe in Fig. 1, particularly for $\nu = (0, 1)$ and $(1, 0)$, where it may also be seen that the joint expectation values collapse on the lines λ_ν after “sliding” in the perpendicular direction towards λ_ν . To understand why this happens, recall that by the same theorem [2], the value of S “drifts” slowly across the zone, i.e., transversely to λ_ν , and is bounded by the zone. So for a reversible drift, the expectation value $\langle S \rangle$ on any resonant eigenstate with given $\langle F \rangle$ should be close to 0, and the corresponding point $(\langle S \rangle, \langle F \rangle)$ lies on the line λ_ν .

Further understanding of the joint expectation value spectrum within the resonant zones can be obtained from the resonant normal forms \mathcal{H}_ν of the Hamiltonian H in Eq. (1). These forms are obtained by averaging with regard to the Hamiltonian flow of

$$\nu \cdot I = \nu_1 I_1 + \nu_2 I_2.$$

Since H is written as a Taylor-Fourier series in action-angle variables, which is customary in this analysis [2], our computations are simplified. Thus the first average simply gives

$$\mathcal{H}_\nu^{(1)} = H_0 + \epsilon V_{(0,0)} + \epsilon V_\nu \quad \text{for } \nu = (1, 0) \text{ and } (0, 1). \quad (5)$$

Using slow-fast variables in Table I, going to the limit of small S near the resonance, and dropping trivial terms that do not contain slow variables (S, σ) , we come to the *pendulum approximation* to the ν -resonant normal form

$$\mathcal{H}_\nu \approx \tilde{\mathcal{H}}_\nu = \frac{1}{2} S^2 + \mathcal{H}_{\text{crit}}(\epsilon, F) \cos \sigma \quad (6)$$

which is commonly encountered in the Nekhoroshev theory. In our case, in this one-dimensional system parameterized by F , the critical energy and the maximum value of $|S|$ attained (when $\sigma = \pi$) on the respective critical orbit (separatrix) are

$$\mathcal{H}_{\text{crit}} = b_\nu(\epsilon) F^2 \quad \text{and} \quad S_{\text{crit}} = \sqrt{2b_\nu(\epsilon)} |F|. \quad (7)$$

They mark the transition between vibrations and rotations and define the boundaries of the resonance zone. For our system, the boundaries are straight lines forming a wedge and the width of the $(1, 0)$ and $(0, 1)$ zones is $\sqrt{\epsilon}$ -small. We draw these wedges in Fig. 1 using Eq. (7) and we can see that Eq. (7) gives a fair estimate of the quantum zones. Resonant quantum states have energies below $\mathcal{H}_{\text{crit}}$ and are rotational (traveling waves) in the F component and vibrational (standing waves) in the S component. Transitional states with energies closely above $\mathcal{H}_{\text{crit}}$ can be seen entering the $(1, 0)$ and $(0, 1)$ zones in Fig. 1. While non-resonant states are nearly degenerate in energy because the dependence on the direction of rotation is relegated to higher orders, the resonant states have this degeneracy removed.

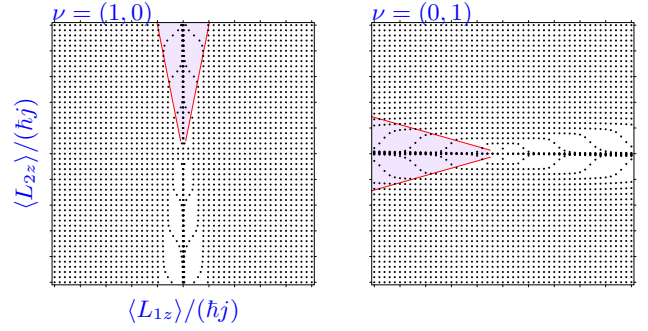


FIG. 2. Joint expectation value spectrum (dots) of \hat{L}_{1z} and \hat{L}_{2z} on the eigenstates of the resonant normal forms $\mathcal{H}_\nu^{(1)}$ in Eq. (5) and classical ν -resonance zones (wedges) for $j = 25$ and $\hbar\epsilon j = 0.005$.

We can verify the precision and the scope of the normal forms in Eq. (5) by using them as quantum Hamiltonians instead of the complete Hamiltonian in Eq. (1). The resulting spectra are shown in Fig. 2. Comparing to Fig. 1, right, we can see that the respective resonant zones are reproduced perfectly, as is the lattice of the nonresonant states. Not surprisingly, the normal forms fail for resonances other than the ones they are designed to describe.

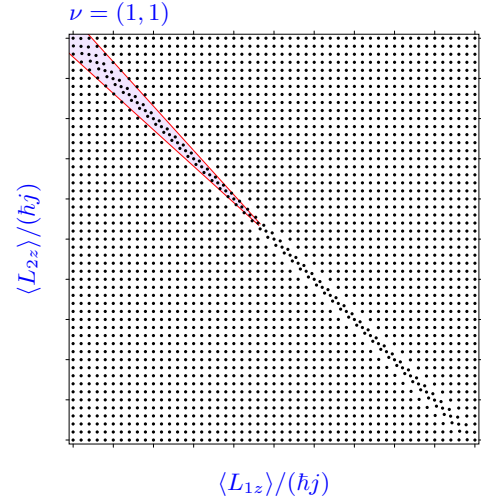


FIG. 3. Joint expectation value spectrum (dots) of \hat{L}_{1z} and \hat{L}_{2z} on the eigenstates of the resonant normal form $\mathcal{H}_{(1,1)}^{(2)}$ in Eq. (8) and the respective classical resonance zone for $j = 25$ and $\hbar\epsilon j = 0.005$.

To compute the normal form for the $(1, 1)$ resonance in our system, we have to go to the second order average

$$\mathcal{H}_{(1,1)}^{(2)} = H_0 + \epsilon V_{(0,0)} + \epsilon^2 V_{(1,1)}^{(2)} \quad (8)$$

where on the assumption $L_{2z} + L_{1z} \approx 0$ (the resonance condition) and to order $O(\sqrt{\epsilon})$ we have

$$V_{(1,1)}^{(2)} \approx 5(L_{2z} - L_{1z})^4 + 12(L_{2z} - L_{1z})^2(L_{1x}L_{2x} - L_{1y}L_{2y}).$$

Introducing slow-fast variables (Table I), fixing F , using S centered on the resonance, and further simplifying for small

224 S , we bring $\mathcal{H}_{(1,1)}^{(2)}$ to the form in Eq. (6), and a similar analy-
 225 sis follows. Note that the width of the (1, 1)-zone of our sys-
 226 tem is ϵ -small. As before, the quantum computation with the
 227 normal form in Eq. (8) shows that this form reproduces per-
 228 fectly the spectrum within its zone. It is instructive to explain
 229 the particular regular pattern we observe.

230 A deeper understanding of the joint expectation value spec-
 231 trum in Fig. 1 calls for a more detailed analysis of the nor-
 232 mal form \mathcal{H} and its pendulum approximation $\tilde{\mathcal{H}}$. While $\tilde{\mathcal{H}}$
 233 does describe the two most important aspects, specifically, the
 234 distinction between the resonant and the non-resonant states
 235 and the boundary of the zone, considering \mathcal{H} as a perturba-
 236 tion of $\tilde{\mathcal{H}}$ becomes essential at medium-to-large $|S|$. Most no-
 237 tably, the perturbation by the $V_{(0,0)}$ term breaks the $S \mapsto -S$
 238 invariance of $\tilde{\mathcal{H}}$ and allows nonzero expectation values $\langle S \rangle$
 239 for large- $|S|$ quasidegenerate doublet states of the pendulum.
 240 There are many ways to treat the perturbation of $\tilde{\mathcal{H}}$ by \mathcal{H} . We
 241 consider briefly a variational study in the basis formed by the
 242 eigenstates $|f, s\rangle$ of \hat{S} and \hat{F} such that

$$\hat{S}|f, s\rangle = \hbar s |f, s\rangle \text{ and } \hat{F}|f, s\rangle = \hbar f |f, s\rangle .$$

243 Note that $|f, s\rangle$ can be easily selected from all states
 244 $|j, m_1\rangle|j, m_2\rangle$ using definitions in Table I. For any fixed f ,
 245 both \mathcal{H} and $\tilde{\mathcal{H}}$ have a tridiagonal matrix in this basis, and a
 246 few basis functions with small $|s|$ may suffice to describe the
 247 patterns in Fig. 1.

248 Thus for the 1:1 resonance, we should consider two pos-
 249 sibilities with half-integer and integer values of s for odd
 250 $|f| < 2j$ and even $|f| \leq 2j$, respectively. In the half-integer
 251 case, the two most resonant states can be approximated by a
 252 2×2 matrix of $\mathcal{H}_{(1,1)}$ in the basis $\{|f, -\frac{1}{2}\rangle, |f, +\frac{1}{2}\rangle\}$

$$\hbar^2 \alpha(f) + \epsilon \hbar^3 \frac{2f^2 + 1}{4} \begin{pmatrix} -1/2 & \epsilon \hbar \pi(f) \\ \epsilon \hbar \pi(f) & +1/2 \end{pmatrix},$$

253 where α and π are smooth functions of (f, j) . Its eigenfunc-
 254 tions have two nonzero $\langle S \rangle$ values on the opposite sides of the
 255 resonance line $\lambda_{(1,1)}$, see Fig. 1. On the other hand, a similar
 256 computation for the integer case using a 3×3 matrix in the ba-
 257 sis with $s = 0, \pm 1$ gives additionally a zero $\langle S \rangle$ value straight
 258 on $\lambda_{(1,1)}$. This describes the joint spectrum near $\lambda_{(1,1)}$. In
 259 simple terms, the particular pattern is due to the alternation
 260 between the integer base which includes the $|f, 0\rangle$ function
 261 and the half-integer base without it.

262 The situation becomes more interesting when the zone is
 263 sufficiently large to capture many states. In our system this
 264 happens for the 1:0 and 0:1 resonances. We find a number
 265 of resonant states with $\langle S \rangle \approx 0$ which are oscillator states
 266 composed of $|f, s\rangle$ with $|s| \ll \hbar^{-1} S_{\text{crit}}$. The $S \mapsto -S$
 267 symmetry of \mathcal{H} can be seen as a dominating factor for them.
 268 The challenge is in reproducing the states with essentially
 269 nonzero $\langle S \rangle$ near S_{crit} , the “wandering states” of the hin-
 270 dered 1-dimensional rotor. As illustrated in Fig. 4, this can be
 271 achieved by taking a sufficiently large number of basis func-
 272 tions with small $|s| \approx \hbar^{-1} S_{\text{crit}}$.

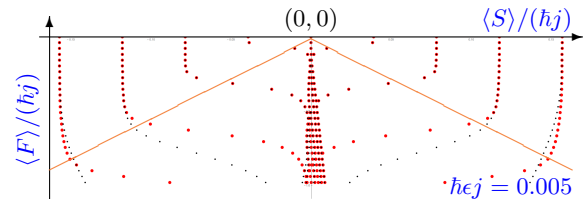


FIG. 4. Joint expectation value spectrum near the 1:0 resonance, cf Fig. 1. Blue dots mark exact $(\langle \hat{L}_{1z} \rangle, \langle \hat{L}_{2z} \rangle)$; larger red circles represent the same values computed for the normal form $\mathcal{H}_{(1,0)}$ in Eq. (5) in the basis of first nine functions $|f, s\rangle$ with $|s| \leq 4$.

TODO: rework this plot (axes, true zone boundaries), make a postscript

274 In this letter, we uncovered basic quantum manifestations
 275 of the classical Nekhoroshev theory and thus provided the
 276 basis to the study of quantum analogs of the resonant and
 277 nonresonant motions in nearly integrable systems, and most
 278 interestingly—of the resonant chaotic dynamics inaccessible
 279 to other frameworks, such as KAM. We can envisage similar
 280 work on perturbations of anisochronous superintegrable sys-
 281 tems with three degrees of freedom, one of the most known
 282 domains of the Nekhoroshev theory. More daringly, for the
 283 resonance zones, we can think of the “Nekhoroshev quanti-
 284 zation” as of a third possibility, a complement to the KAM-
 285 inspired Einstein–Brillouin–Keller (EBK) torus quantization
 286 and the periodic orbit (PO) quantization (Van Vleck, Gutzwil-
 287 ler, Feynman), where fast actions F can be quantized within
 288 the EBK approach, while the dynamics in the slow actions S
 289 is treated using the semiclassical PO methods.

290 D. Fontanari is grateful for the support by the two universities
 291 and the province of Trentino during his PhD thesis [7].

* Electronic mail: fontanari@purple.univ-littoral.fr

† Electronic mail: fasso@math.unipd.it

‡ Corresponding author: sadovskii@univ-littoral.fr

- [1] N. N. Nekhoroshev, in *Proceedings of the International Congress of Mathematicians: Vancouver, B.C., Aug. 21–29, 1974*, edited by R. D. James (Canadian Mathematical Congress, Montreal, Quebec, Canada, 1975) pp. 309–314, (spelled Nekhoroshev).
- [2] N. N. Nekhoroshev, *Russ. Math. Surv.* **32**, 1 (1977).
- [3] J. Laskar, in *Hamiltonian Systems with Three or More Degrees of Freedom*, NATO ASI Series, Vol. 533, edited by C. Simó (Springer Verlag, Netherlands, 1999) pp. 134–150.
- [4] H. S. Dumas and J. Laskar, *Phys. Rev. Lett.* **70**, 2975 (1993).
- [5] S. B. Kuksin and A. I. Neishtadt, *Russ. Math. Surv.* **68**, 335 (2013).
- [6] C. Chandre, J. Laskar, G. Benfatto, and H. Jauslin, *Physica D* **154**, 159 (2001).
- [7] D. Fontanari, *Quantum manifestations of the adiabatic chaos in perturbed superintegrable Hamiltonian systems*, Ph.D. thesis, Università di Padova / Université du Littoral, Padova (2013).

- 312 [8] N. N. Nekhoroshev, *Functional Anal. Appl.* **5**, 338 (1971). 316 [11] F. Fassò and G. Benettin, *ZAMP* **40**, 307 (1989).
313 [9] N. N. Nekhoroshev, *Trudy Sem. I. G. Petrovskogo* **5** (1979), in 317 [12] P. Lochak, *Russ. Math. Surveys* **47**, 57 (1992).
314 Russian, 46p.
315 [10] G. Benettin and G. Gallavotti, *J. Stat. Phys.* **44**, 293 (1986).